



# Repair of osteochondral defects mediated by double-layer scaffolds with natural osteochondral-biomimetic microenvironment and interface



Tao Wang<sup>a,c,1</sup>, Wei Xu<sup>a,c,1</sup>, Xintong Zhao<sup>b,c,1</sup>, Baoshuai Bai<sup>a,c</sup>, Yuejie Hua<sup>b,c</sup>, Jincheng Tang<sup>a,c</sup>, Feifan Chen<sup>a,c</sup>, Yu Liu<sup>b,c</sup>, Yahui Wang<sup>c,\*\*</sup>, Guangdong Zhou<sup>a,b,c,\*\*\*</sup>, Yilin Cao<sup>a,b,c,\*</sup>

<sup>a</sup> Research Institute of Plastic Surgery, Wei Fang Medical University, Wei Fang, Shandong, 261041, PR China

<sup>b</sup> Department of Plastic and Reconstructive Surgery, Shanghai Ninth People's Hospital, Shanghai Jiao Tong University School of Medicine, Shanghai Key Laboratory of Tissue Engineering, Shanghai, 200011, PR China

<sup>c</sup> National Tissue Engineering Center of China, Shanghai, 200241, PR China

## ARTICLE INFO

### Keywords:

Laser technology  
Acellular osteochondral matrix  
Biomimetic scaffold  
Hydrogel  
Osteochondral defect

## ABSTRACT

Tissue engineering provides a new approach for the treatment of osteochondral defects. However, the lack of an ideal double-layer scaffold with osteochondral-biomimetic microenvironment and interface similar to native articular tissue greatly limits clinical translation. Our current study developed a double-layer acellular osteochondral matrix (AOM) scaffold with natural osteochondral-biomimetic microenvironment and interface by integrating ultraviolet (UV) laser and decellularization techniques. The laser parameters were optimized to achieve a proper pore depth close to the osteochondral interface, which guaranteed complete decellularization, sufficient space for cell loading, and relative independence of the chondrogenic and osteogenic microenvironments. Gelatin-methacryloyl (GelMA) hydrogel was further used as the cell carrier to significantly enhance the efficiency and homogeneity of cell loading in the AOM scaffold with large pore structure. Additionally, *in vitro* results demonstrated that the components of the AOM scaffold could efficiently regulate the chondrogenic/osteogenic differentiations of bone marrow stromal cells (BMSCs) by activating the chondrogenic/osteogenic related pathways. Importantly, the AOM scaffolds combined with BMSC-laden GelMA hydrogel successfully realized tissue-specific repair of the osteochondral defects in a knee joint model of rabbit. The current study developed a novel double-layer osteochondral biomimetic scaffold and feasible strategy, providing strong support for the tissue-specific repair of osteochondral defects and its future clinical translation.

## 1. Introduction

Trauma, aging, and disease easily lead to articular cartilage defects, which are usually accompanied by a subchondral bone defect. The repair of osteochondral defects is always an intractable problem in clinical practice. At present, the current clinical treatment methods for physiological repair and regeneration of osteochondral defects mainly include microfractures [1–3], autologous chondrocyte transplantation [4,5], and autologous osteochondral grafts [2,6,7]. However, the treatments either achieve limited repair effects with inferior tissue integration or lack

sufficient autologous graft that is associated with injury to a donor site [8, 9]. Tissue engineering provides a new direction for the treatment of osteochondral defects, which benefit from autologous living osteochondral tissue that is hopefully regenerated by combining with autologous cells and a biodegradable scaffold [10–12]. Although there were a few osteochondral systems, such as MaioRegen (a scaffold composed of collagen and hydroxyapatite) and Agili-C™ (a scaffold based on aragonite), have been reported clinical improvements (significant improvement in IKDC and Tegner scores) after more than 3 years follow-up [13, 14], it was hard to prepare an ideal double-layer scaffold with natural

\*Corresponding author. Department of Plastic and Reconstructive Surgery, Shanghai Ninth People's Hospital, Shanghai Jiao Tong University School of Medicine, Shanghai Key Laboratory of Tissue Engineering, Shanghai, 200011, PR China.

\*\* Corresponding author. National Tissue Engineering Center of China, Shanghai, 200241, PR China.

\*\*\* Corresponding author. Department of Plastic and Reconstructive Surgery, Shanghai Ninth People's Hospital, Shanghai Jiao Tong University School of Medicine, Shanghai Key Laboratory of Tissue Engineering, Shanghai, 200011, PR China.

E-mail addresses: [yahuiwang10@163.com](mailto:yahuiwang10@163.com) (Y. Wang), [guangdongzhou@126.com](mailto:guangdongzhou@126.com) (G. Zhou), [yilincao163@163.com](mailto:yilincao163@163.com) (Y. Cao).

<sup>1</sup> These authors contributed equally to this work.

osteocondral-biomimetic microenvironment and interface similar to native articular tissue.

To solve the above problem, the key challenge is preparing an ideal double-layer scaffold. Such a double-layer scaffold should simultaneously meet the following requirements: 1) biomimetic chondrogenic microenvironment and structure of the cartilage layer for supporting cartilage regeneration [15–17]; 2) biomimetic osteogenic microenvironment and structure of the bone layer for supporting bone regeneration [18–21]; 3) biomimetic interface between the cartilage layer and bone layer similar to the native osteochondral interface [22–25]; 4) high mechanical strength suitable for surgical operation and immediate function maintenance [26–30]; and 5) a biomimetic three dimensional (3D) morphology that matches the osteochondral defect. Apparently, it is very difficult to prepare such a challenging scaffold with the above multiple requirements via artificial synthesis. The development of acellular technology provides a new strategy for the preparation of a natural biomimetic scaffold [31]. Theoretically, acellular osteochondral matrix (AOM) scaffold based on natural osteochondral tissue is hopefully to simultaneously meet all of the above requirements. However, there have been no reports on whether natural osteochondral tissue can be prepared into an AOM scaffold suitable for cell loading and tissue-specific repair.

To successfully prepare such an AOM scaffold for tissue-specific repair of osteochondral defects, the following challenges and questions should be solved and clarified: 1) How to prepare a porous AOM scaffold with natural interface and biphasic osteochondral microenvironment? 2) Can the AOM scaffold achieve high cell seeding efficiency? If not, how to solve this problem? 3) Whether the AOM scaffold has the ability of accurate biphasic regulation for both chondrogenic and osteogenic differentiation? What are the possible mechanisms? 4) Whether the cell-scaffold constructs can achieve satisfactory tissue-specific repair of osteochondral defects?

To address the above questions, we proposed a novel strategy for preparing an AOM scaffold. The porous structure of bone tissue was easier to achieve decellularization and cell loading [32], while the dense and imporous structure of articular cartilage limited the efficiency of decellularization and cell loading [33]. Although this intractable problem could be solved by freezing grinding and cutting into thin slices [15, 34], it was greatly destroyed the structure of natural cartilage and had low mechanical strength, which was not conducive to clinical transformation. In current research, the application of UV picosecond laser drilling technology to generate a porous structure in the cartilage layer of the osteochondral tissue likely a promising approach to solve this challenge, while still maintained basic structure of natural cartilage and high mechanical properties. The depth of the micropores was optimized to ensure the integrity of the natural interface between the cartilage layer and bone layer, so that the relatively independent microenvironment in the cartilage layer and bone layer did not interfere with each other during osteochondral repair *in vivo*. Then, GelMA hydrogel was used as a cell carrier to enhance the cell seeding efficiency in the oversize pores (both the artificial micropores in the cartilage layer and the native bone trabecular interval in the bone layer) of AOM scaffold. In addition, the tissue-specific induction ability of AOM scaffold for bone marrow stromal cells (BMSCs) and potential mechanisms were also investigated *in vitro*. Finally, the AOM scaffolds combined with BMSC-laden GelMA hydrogel were implanted *in vivo* to explore the feasibility of tissue-specific repair of osteochondral defects. The current study developed a novel biomimetic microenvironment scaffold with osteochondral biphasic regulation for BMSCs and provided a novel strategy for tissue-specific repair of osteochondral defects.

## 2. Materials and methods

### 2.1. Preparation of materials

**Preparation of the AOM scaffold:** Porcine knee joints were purchased from Shanghai Jiagan Experimental Animal Raising Farm

(Shanghai, China). Osteochondral tissues with a cylindrical shape were obtained from the femoral condyle using a bone drill (inner diameter 4 mm). The thickness of the cartilage layer was cut to approximately 1 mm and the thickness of the bone layer was cut to approximately 2 mm. All of the animal procedures were approved by the Animal Care and Experiment Committee of Shanghai Jiao Tong University School of Medicine (SH9H-2021-A655-SB). The osteochondral tissues were then placed in the Ultraviolet Picosecond Laser Machine (PX100-3-GF, Edgewave, North Rhine-Westphalia, Germany) with the cartilage layer facing up. The laser parameters were set to 88% power and 400 KHz, and the laser repetitions (10, 15, and 20) were adjusted to optimize the depth and diameter of the cartilage layer micropores. AOM scaffold were obtained after the decellularization process using previously reported method with some modification [35]. Fresh osteochondral samples were sequentially treated in a shaking table (37 °C, 120 rpm) with 0.25% trypsin in Phosphate-Buffered Saline (PBS) solution for 24 h, nuclease solution (40 U/ml DNase and 1 U/ml RNase A in 10 mM Tris-HCL, PH = 7.5) for 12 h, hypotonic Tris-HCL solution for 24 h, and 1% Triton X-100 solution (v/v) for 24 h. Finally, all the samples were washed in PBS solution for 24 h to obtain the AOM scaffolds, which were stored at –20 °C for subsequent use. All solutions used in the decellularization process were replaced with the fresh one at every 6 h.

**Preparation of GelMA hydrogel:** GelMA hydrogel was prepared as described in the previous study [36,37]. Briefly, GelMA was synthesized by the reaction of gelatin (from porcine skin) with methacrylic anhydride (MA). MA was added to prepare a solution of gelatin with vigorous stirring until completely dissolved. After reacting for 3 h, the mixture was dialyzed against distilled water for 1 week at 40 °C and then freeze-dried to obtain the white porous foam-like GelMA prepolymer. Finally, freeze-dried GelMA at concentrations of 7% (w/v) was dissolved in PBS solution with 0.15% (w/v) lithium phenyl-2,4,6-trimethylbenzoylphosphinate (LAP) photo initiator [38].

### 2.2. Characterization of materials

**Scanning electron microscopy (SEM):** The samples from the osteochondral tissues, AOM scaffolds, and BMSC-laden AOM constructs were immobilized in 0.05% glutaraldehyde and dehydrated in a series of ethanol solutions. After dried and gold-sputtered, the samples were observed by SEM (JSM6490, JEOL, Kyoto, Japan) at an accelerating voltage of 15 kV.

**Decellularization effect assessment of the AOM scaffold:** Hematoxylin and eosin (HE) staining, 4',6-diamidino-2-phenylindole (DAPI) staining, and DNA quantitative analysis were used to evaluate whether the cells were removed completely in the AOM scaffold [15]. Then, the glycosaminoglycan (GAG) content, total collagen content, and mechanical strength of the samples before and after acellularization were quantitatively analyzed [15,39]. Galactose- $\alpha$ -1,3-galactose (alpha-gal) content of the samples before and after decellularization was examined by using antigen quantitative detection kit (70101, Sanyao Science, China) according to the method provided by the manufacturer.

**Characterization of GelMA hydrogel and GelMA-AOM:** Rheology test of pure GelMA hydrogel was analyzed on a HAAKE MARS III photo rheometer with a parallel-plate (P20 TiL, 20 mm diameter) and 365 nm light irradiation (50 mW/cm<sup>2</sup>) at 37 °C [40]. Swelling, degradation, and mechanical strength tests of the pure GelMA hydrogel and GelMA-AOM (GelMA hydrogel inoculated into AOM scaffold) samples were evaluated after 365 nm light irradiation in accordance with previously reported methods with some modifications [15,41,42]. Briefly, the samples were fully immersed in PBS solution (37 °C, pH = 7.4) to perform the swelling test. The samples were fully immersed in PBS solution (pH = 7.4) containing 0.15% (w/v) collagenase (Worthington Biochemical Corp., Freehold, NJ, USA) to perform the degradation test (placed in a shaking table, 37 °C, 120 rpm). Samples were prepared as cylindrical shapes for the Young's modulus test [15].

### 2.3. Preparation of cell-scaffold constructs

**Isolation and culture of BMSCs:** Twenty-four healthy New Zealand rabbits weighing 2.5 kg–3 kg were used to obtain bone marrow aspirate, which was then cultured for 5 days without changing the culture medium to promote cell adhesion on the culture dish. The isolated BMSCs were cultured in Dulbecco's Modified Eagle Medium (DMEM; Gibco, Grand Island, NY) supplemented with 10% fetal bovine serum (FBS; Hyclone, Logan, UT, USA) and 1% penicillin/streptomycin at 37 °C with 5% CO<sub>2</sub> [43].

**Cell seeding:** AOM scaffolds were sterilized under an electron accelerator (dose = 25 kGy) before cell seeding. In the GelMA group, BMSCs were suspended by the GelMA hydrogel (cell density =  $30 \times 10^6$  cells/mL) to inoculate the AOM scaffolds under mild negative pressure. The constructs of the GelMA group were irradiated with 365 nm light until the GelMA hydrogel solidified. In the Control group, BMSCs in the conventional DMEM medium were seeded on the AOM scaffolds under mild negative pressure, and then incubated for 4 h at 37 °C. Finally, all constructs of the two groups were cultured in DMEM medium containing 10% FBS and 1% penicillin/streptomycin at 37 °C with 5% CO<sub>2</sub>.

### 2.4. Biocompatibility of the AOM scaffold

**Gross observation:** Macroscopic and SEM images were used to observe appearance changes of the constructs from the Control group and GelMA group after 1-, 4-, and 7-days *in vitro* culture, including the cartilage layer (Front view) and bone layer (Reverse view).

**Cell seeding efficiency:** The cell seeding efficiency was measured after 24 h of *in vitro* culture, the constructs from two groups were gently washed with PBS to remove dead cells. The number of cells in the washing solution and petri dish were denoted by N. The cell seeding efficiency of the AOM scaffold was calculated using the following formula:  $((\text{Total number of cells} - N) / \text{Total number of cells}) \times 100\%$ .

**Cell viability test:** After *in vitro* culture for 1, 4, and 7 days, the constructs from GelMA group and Control group were observed under confocal microscopy (Nikon, Tokyo, Japan) using Live & Dead cell staining (Invitrogen, Carlsbad, CA, USA) in accordance with the manufacturer's instructions.

**Cell proliferation test:** After *in vitro* culture for 1, 4, and 7 days, the total DNA was extracted from the constructs and quantitatively analyzed using the PicoGreen dsDNA assay (Invitrogen, Carlsbad, CA, USA) based on the above protocols [15].

**Cytotoxicity of AOM scaffold:** BMSCs were seeded at a density of  $2 \times 10^4$ /mL in the extract solutions (supernatant from AOM scaffold soaked in DMEM for 72 h) regular DMEM medium for 7 days. In accordance with the manufacturer's instructions, the Cell Count Kit-8 (CCK-8; Dojindo, Kumamoto, Japan) was used to measure the cytotoxicity of the scaffold and the value was expressed by the average optical density (OD) of 5 holes.

### 2.5. Tissue-specific differentiation of BMSCs induced by AOM scaffold

***In vitro* induction of BMSCs by the components of the AOM scaffold:** The AOM scaffold was incised along the interface to separate the cartilage layer from the bone layer. After grinding, acellular cartilage matrix (ACM) powder and acellular bone matrix (ABM) powder were obtained. Then, BMSCs were *in vitro* culture for 14 days in ACM-added medium (ACM group) for chondrogenic differentiation and medium with ABM-added (ABM group) for osteogenic differentiation. In addition, BMSCs were cultured in medium without powder was set as the Control group.

**Immunofluorescence staining:** For immunofluorescence assay, the positive expression (red color) of Type II collagen (COL II) and Type I collagen (COL I) was detected to further confirm cartilage-specific and bone-specific phenotype, respectively, after tissue-specificity induction. Meanwhile, DAPI staining was used to detect nuclei [44].

**Quantitative reverse transcription polymerase chain reaction (qRT-PCR):** In accordance with the previous method [45], BMSCs of each group were digested after *in vitro* culture for 14 days. Then expression level of cartilage-related genes, such as COL II, aggrecan (ACAN), and SOX9 were evaluated in the Control group and ACM group. Similarly, bone-related genes, such as COL I, ALP, and osteocalcin (OCN) were evaluated in the Control group and ABM group.

**RNA sequencing (RNA-seq) analysis:** For RNA-seq analysis, the total RNA was extracted from the BMSCs using TRIzol Reagent (Invitrogen, Carlsbad, CA, USA), after *in vitro* culture for 14 days. The TruSeq™ RNA Sample Preparation Kit (Illumina, San Diego, CA, USA) was used to establish the library. The Illumina HiSeq XTEN/NovaSeq 6000 sequencing platform was then used for high-throughput sequencing of the library. The mapped reads were assembled by StringTie. To identify the differentially expressed genes (DEGs), the expression level of each transcript was calculated by transcripts per million reads (TPM). Finally, Kyoto Encyclopedia of Genes and Genomes (KEGG) pathway analysis and Gene Ontology (GO) functional enrichment were carried out by Goatoools and KOBAS.

### 2.6. Repair of osteochondral defects

In this study, twenty-four healthy New Zealand rabbits (4 months old) weighing 2.5 kg–3 kg were used in the defect models. All animals were randomly divided into three groups: defects without treatment (Untreated group), defects filled with AOM scaffolds combined with GelMA hydrogel (Control group), and defects filled with AOM scaffolds combined with BMSC-laden GelMA hydrogel (Experimental group). After opening the knee joint, a stainless-steel drill was used to create an osteochondral defect with a diameter of 4 mm and a depth of 3 mm at the pulley. The rabbits were euthanized after 6 weeks and 12 weeks post-implantation.

### 2.7. Gross observation and micro-CT analysis

After euthanizing the animals at 6 weeks and 12 weeks, the International Cartilage Repair Society (ICRS) macroscopic assessment scale was used to evaluate the effect of cartilage repair [46]. The samples were then placed in 4% (w/v) paraformaldehyde buffer for 2 days and micro-CT analysis was performed using a micro-CT  $\mu$ 80 scanner (Scanco Medical, Switzerland). The scanning parameters were set as follows: voltage = 70 kV, current = 114  $\mu$ A, resolution =  $1024 \times 1024$  pixels. Evaluation software (Scanco Medical, Switzerland) was used for data analysis and 3D image reconstruction. Micro-CT analysis was conducted to acquire 3D reconstruction images and two dimensional (2D) cross-sectional images, which were calculated to obtain the relative bone volume fraction (BV/TV), bone mineral density (BMD), and trabecular thickness (Tb. Th) quantitative data.

### 2.8. Gene expression and histological analysis

Twelve weeks post-implantation, the expression levels of COL I, COL II, ACAN, and OCN in the repair region of the three groups were analyzed based on the method described in previous study [47]. HE, Safranin-Fast green (S-F), and Masson's-Trichrome (M-T) were conducted to evaluate the osteochondral repair effect by acquiring microscopic images. Immunohistochemical (IHC) staining of COL I and COL II was conducted to confirm cartilage-specific and bone-specific proteins [48,49], respectively, in the osteochondral defect region. The expression of collagen I and collagen II were detected using rabbit polyclonal antibody (ab233080, abcam, Cambridge, USA) and (ab34712, abcam, Cambridge, USA), respectively. Finally, the samples were evaluated using the O'Driscoll histological assessment scale [50].

## 2.9. Statistical analysis

All data were collected from at least three repetitions. The data are presented as the means  $\pm$  SD. One-way analysis of variance was used to evaluate the statistically significant differences between groups, and  $*P < 0.05$  was considered statistically significant.

## 3. Results

### 3.1. Preparation of AOM scaffold

As shown in Fig. 1, control of the porous structure of the cartilage layer was the first step and important pretreatment for the preparation of AOM scaffold. As shown in Fig. 2, the natural osteochondral tissue comprised a dense cartilage layer and porous cancellous bone layer with a dense and continuous interface between them (Fig. 2A1). After laser drilling, homogeneously distributed U-shaped porous structures were distinctly observed in the cartilage layer (Fig. 2B1). As the number of laser repetitions increased, the diameter and depth of the U-shaped micropores increased gradually (Fig. 2E–F). At 10 laser repeats, the depth of the micropores only reached approximately 700  $\mu\text{m}$ , which was far away from the interface of the cartilage and bone (Fig. 2B3, B4). At 15 laser repeats, the depth of micropores reached approximately 900  $\mu\text{m}$ , which was very close to, but did not damage, the interface (Fig. 2C3, C4). At 20 laser repeats, the depth of the micropores reached more than 1300  $\mu\text{m}$ , which badly destroyed the interface (Fig. 2D3, D4). Collectively, 15 repeats of laser drilling were the relatively optimized parameter for control of the porous structure of the cartilage layer that facilitated decellularization treatment, provided sufficient space for cell loading, and maintained relative independence of the chondrogenic and osteogenic microenvironments.

The decellularized treatment was the essential step for decreasing the immunogenicity of the AOM scaffold. As shown in Figure S1, both the gross view and SEM images showed that the decellularized treatment did not have a significant influence on the double-layer structure, micropore structures, or the interface of AOM scaffolds. Histologically, HE staining showed that abundant cell structures with distinct nuclei were observed

in both the cartilage layer and bone layer (Fig. 3A1, C1); however, only empty cartilage and bone lacunae were observed after the decellularized treatment (Fig. 3B1, D1). DAPI staining further confirmed that the abundant cell nuclei with blue fluorescence in the natural osteochondral tissue (Fig. 3A2, C2) completely disappeared in both the cartilage layer and bone layer after decellularization (Fig. 3B2, D2). SEM images revealed that the lacuna structures containing cells were observed in the natural cartilage layer, while obvious empty lacunae were observed after decellularization (Fig. 3A3, B3). No obvious differences were observed in the SEM images of the bone layer before and after decellularization, likely because of the influence of the abundant mineralized matrices (Fig. 3C3, D3). DNA quantitative analysis further confirmed that the DNA content decreased from approximately 164.0 ng/mg to approximately 11.8 ng/mg (more than 92% of the DNA was removed) after decellularized treatment (Fig. 3E). After the decellularization, alpha-gal quantitative analysis showed that the alpha-gal content was decreased from approximately 8.6 U/mg to approximately 1.7 U/mg (more than 80% was removed) (Fig. 3F). The removal of most of the DNA and alpha-gal content was conducive to the reduction of immune rejection after xenografts transplantation in the future clinical translation. Quantitative analyses of the extracellular matrix (ECM) demonstrated that the GAG content in the cartilage layer of AOM scaffolds decreased from approximately 48.1 mg/g to approximately 36.1 mg/g (maintained approximately 75% of the native level) (Fig. 3G). Similarly, the total collagen content in the cartilage layer of AOM scaffolds decreased from approximately 3.6 mg/g to approximately 3.0 mg/g (maintained approximately 83% of the native level) (Fig. 3H). Importantly, compare to the native level (approximately 13 MPa), the Young's modulus of the acellular cartilage layer in the AOM scaffolds still maintained approximately 8.3 MPa (maintained approximately 63% of the native level) after decellularization (Fig. 3I), which provided sufficient mechanical strength for surgical operation and immediate function maintenance during the repair of osteochondral defects. All of these results indicated that the AOM scaffolds basically retained the main bioactive components of the cartilage layer (such as GAG and collagen) with high mechanical strength and low immunogenicity.

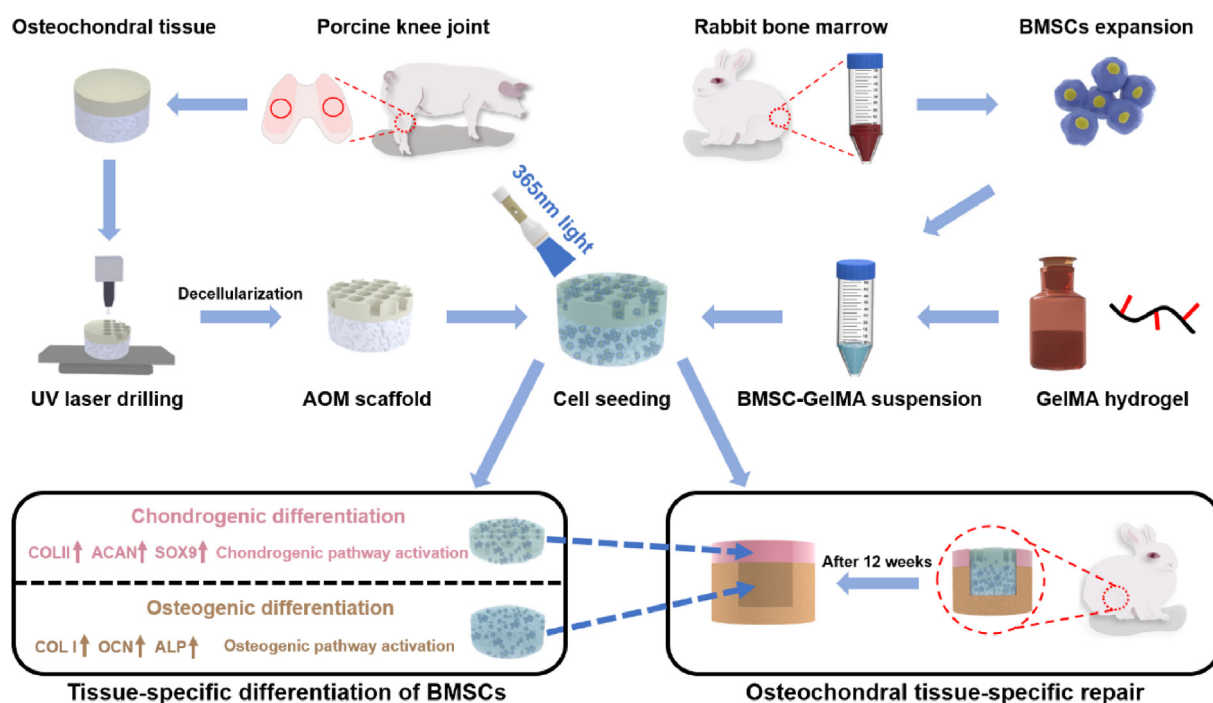
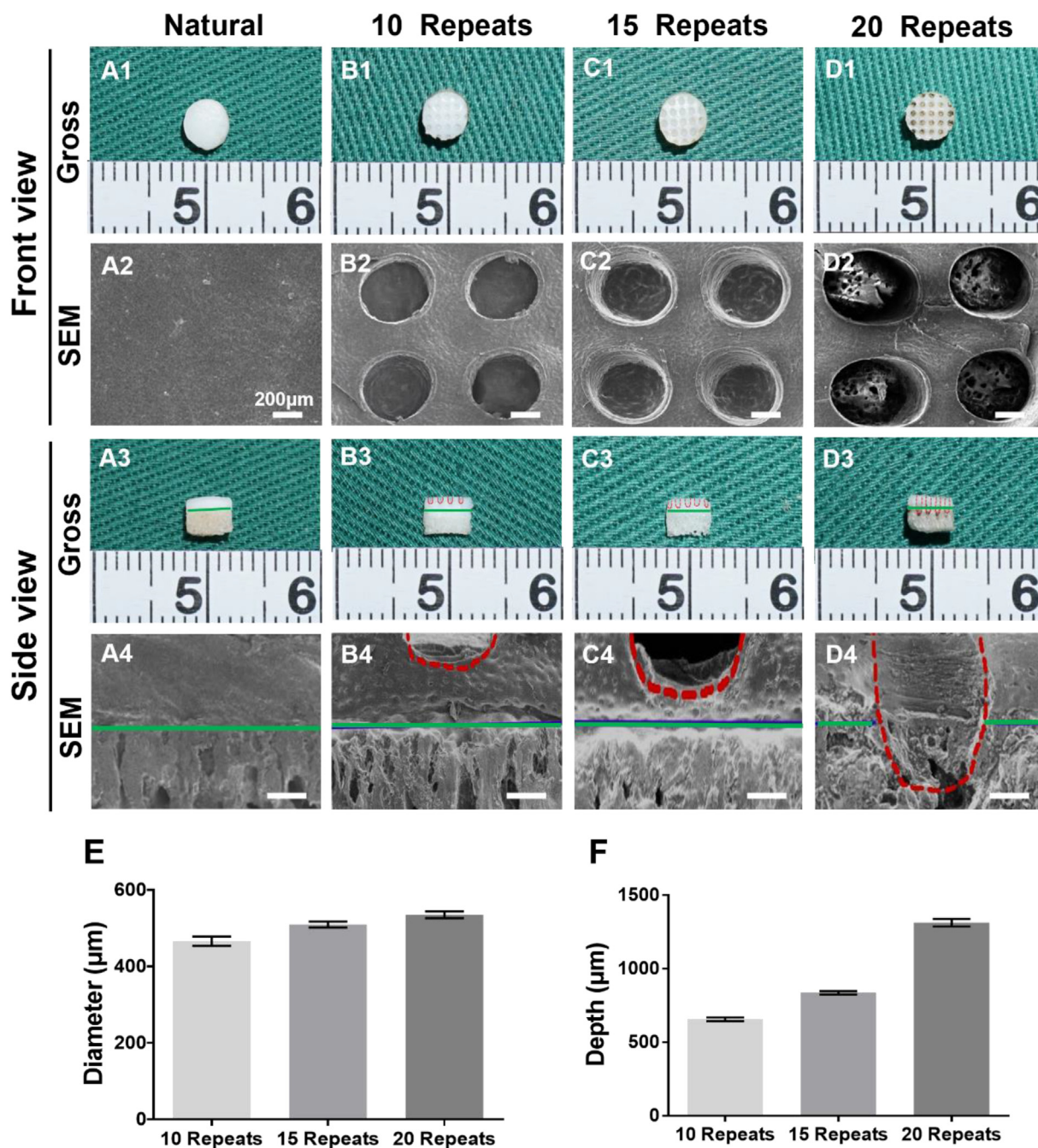


Fig. 1. Schematic illustration of the preparation of the AOM scaffold and BMSC-GelMA suspension for osteochondral tissue-specific repair. UV: ultraviolet. AOM: acellular osteochondral matrix. BMSC: bone marrow stromal cell. GelMA: Gelatin-methacryloyl.



**Fig. 2. Optimization of the laser drilling parameters for porous structure control of the cartilage layer.** (A1-A4) Natural osteochondral tissue with a dense cartilage layer before laser drilling. (B1-D4) Homogeneously distributed U-shaped porous structures are observed in the cartilage layer after laser drilling and different laser repetition times lead to different diameters and depths of the micropores. The (E) diameter and (F) depth of the micropores increase gradually with the increase of laser repetitions. The red dotted lines indicate the outline of the micropores and the solid green lines indicate the interface between the cartilage layer and bone layer. (n = 4).

### 3.2. *In vitro* evaluation of GelMA hydrogel and AOM scaffold

The characteristics of the GelMA hydrogel integrating with the AOM scaffold were first investigated to predict the feasibility of the GelMA hydrogel as a cell carrier for cell loading of AOM scaffold. As shown in our results, the GelMA hydrogel showed excellent photocuring performance with a fast gelation time of approximately 5s under *in situ* 365 nm light irradiation (Figure S2A1-A5, C). GelMA hydrogel could easily enter the pores of the AOM scaffold under a mild negative pressure condition (Figure S2B1, B2). After light irradiation, the GelMA hydrogel rapidly solidified and filled the porous structures of both the acellular cartilage

layer and acellular bone layer in the AOM scaffold (Figure S2B4-B5), predicting that the GelMA hydrogel was probably an eligible cell carrier for cell loading of the AOM scaffold. The swelling and degradation ratio of the GelMA-AOM samples were significantly less than those of the pure GelMA hydrogel (Figure S2D, E), which was mainly attributed to the relatively solid structure and natural ECM components of the AOM scaffolds. The mechanical analysis showed that the Young's moduli of both the AOM scaffolds and GelMA-AOM constructs were significantly greater than that of the GelMA hydrogel (after gelation) and the addition of the GelMA hydrogel in the AOM scaffolds slightly enhanced the Young's moduli of the samples (Figure S2F).

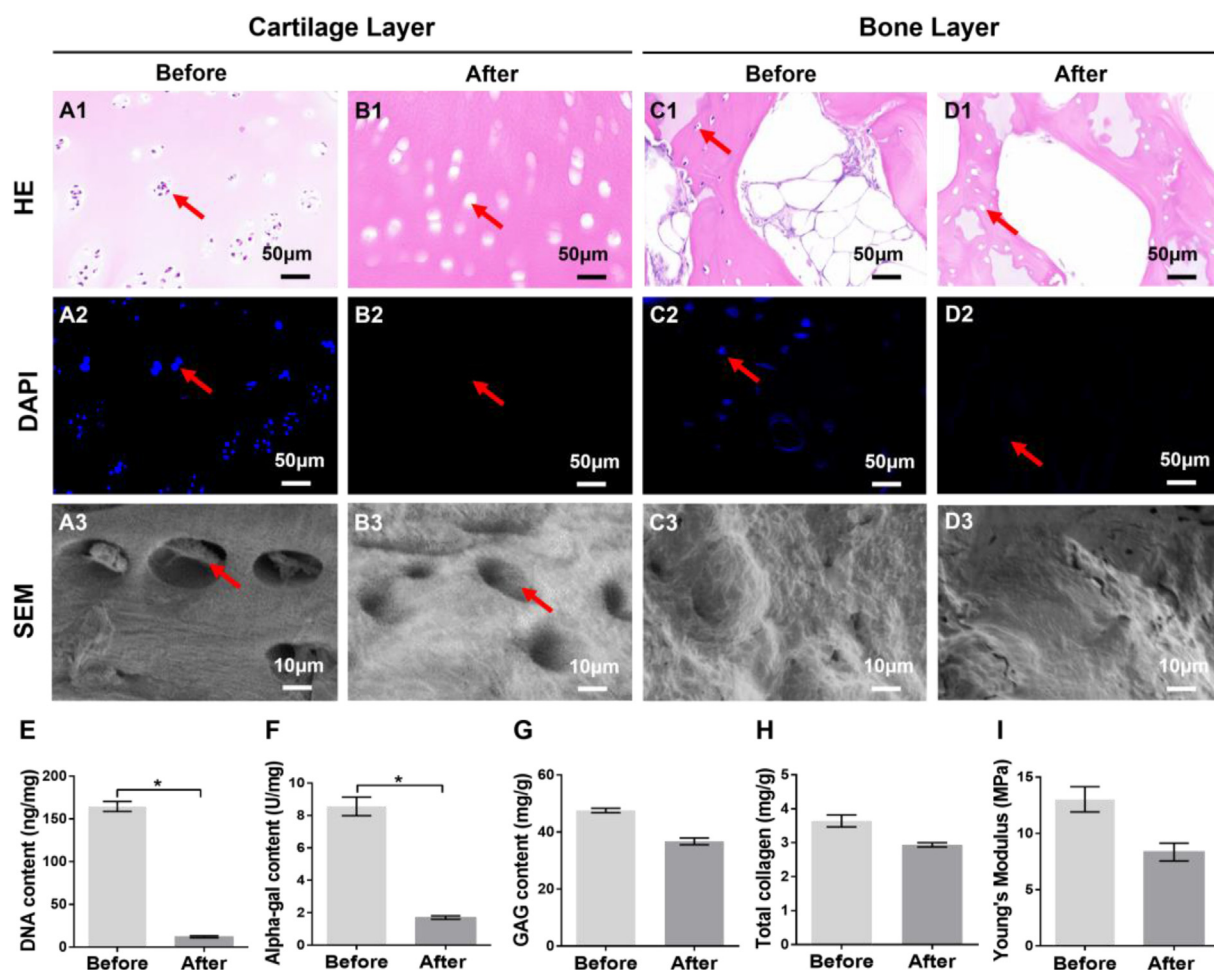


**Fig. 3.** The qualitative and quantitative evaluations of the AOM scaffold. (A1–A3) Cartilage layer of the osteochondral tissue before decellularization. (B1–B3) Cartilage layer of the AOM scaffold after decellularization. (C1–C3) Bone layer of the osteochondral tissue before decellularization. (D1–D3) Bone layer of the AOM scaffold after decellularization. Quantitative analyses of the (E) DNA content, (F) alpha-gal content, (G) GAG content, (H) total collagen content, and (I) Young's modulus before and after decellularization. The red arrows indicate the presence and absence of cell nuclei before and after decellularization. (n = 4).

The BMSC-laden GelMA hydrogel was seeded into the AOM scaffolds to further confirm the feasibility and biocompatibility of the GelMA hydrogel served as a cell carrier for cell loading of the AOM scaffolds. As shown in Fig. 4A1–A6, the BMSC-laden GelMA hydrogel retained the fast gelation characteristic of the GelMA hydrogel, filled the porous structures of both the acellular cartilage layer and acellular bone layer, and integrated well with the AOM scaffolds without obvious loss during the *in vitro* culture. The SEM images further revealed that the pores in both the acellular cartilage layer and acellular bone layer were filled well with the BMSC-laden GelMA in the GelMA group (Fig. 4B1–B6). Live & Dead cell staining showed that the BMSCs grew well with relatively homogeneous distribution on the AOM scaffolds in the GelMA group (Fig. 4C1–C6). Alternatively, the porous structure of the Control group with conventional cell loading was distinctly observed in both the acellular cartilage layer and acellular bone layer (Fig. 4D1–E6). Live & Dead cell staining also showed that the number of BMSCs in the Control group was much less than that in the GelMA group (Fig. 4F1–F6). Notably, homogeneously distributed acellular regions similar to the pore of AOM scaffold were distinctly observed in the Control group, which was attributed to the lack of cell carrier in the central regions of the pores (Fig. 4F1–F6).

Quantitative analyses further demonstrated that the cell seeding efficiency in the GelMA group reached nearly 100% (Fig. 4G) and the DNA content significantly increased with the culture time (Fig. 4H), which were significantly greater than those in the Control group, indicating that BMSCs could be well fixed into AOM scaffolds by solidified GelMA

hydrogel and that the GelMA hydrogel had eligible biocompatibility for supporting cell proliferation. The cytotoxicity test verified that the extract solutions of the AOM scaffold had no negative effect on the survival and proliferation of BMSCs (Fig. 4I). These results demonstrated that the integration of the GelMA hydrogel and AOM scaffold was an excellent strategy for supporting cell loading, homogeneous distribution, fixation, and proliferation. Therefore, we used this strategy (the integration of the GelMA hydrogel and AOM scaffold) for the subsequent *in vivo* experiments of rabbit knee osteochondral defects.

### 3.3. Tissue-specific differentiations induced by the AOM scaffold

The roles of the AOM scaffold in regulating chondrogenic and osteogenic differentiations of BMSCs were further detected by an immunofluorescence and qRT-PCR assay. The results showed that the addition of ACM powder derived from the acellular cartilage layer of the AOM scaffold in the culture system obviously promoted the expression of COL II (Fig. 5A) and significantly up-regulated the expression of cartilage-specific genes (COL II, ACAN, and SOX9) (Fig. 5C), indicating a strong chondrogenic-induced role of acellular cartilage layer in the AOM scaffold. Meanwhile, the addition of the ABM powder derived from the acellular bone layer of the AOM scaffold in the culture system could obviously promote the expression of COL I (Fig. 5B) and significantly up-regulate the expression of bone-specific genes (COL I, ALP, and OCN) (Fig. 5D), indicating a strong osteogenic-induced role of the acellular

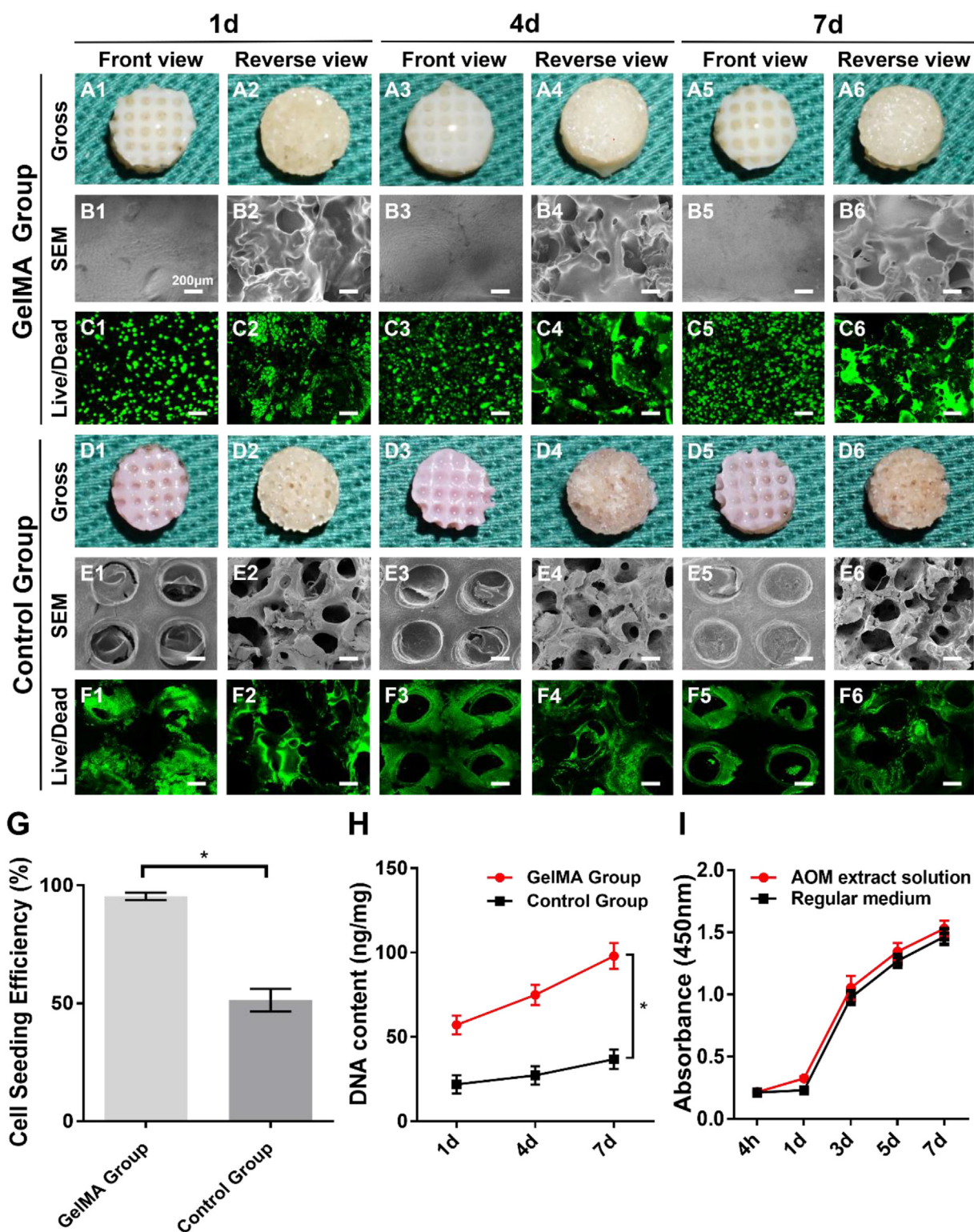


**Fig. 4.** Biocompatibility evaluation of the GelMA hydrogel and AOM scaffold. (A1–A6) Gross observations of the GelMA group after cell loading at 1, 4, and 7 days. (B1–B6) SEM images of the GelMA group at the above time points. (C1–C6) Live & Dead cell staining of the GelMA group at the above time points. (D1–D6) Gross observations of the Control group at the above time points. (E1–E6) SEM images of the Control group at the above time points. (F1–F6) Live & Dead cell staining of the Control group at the above time points. The quantitative analyses of (G) cell seeding efficiency and (H) DNA content in the GelMA and Control groups. (I) Cytotoxicity test for the AOM scaffold. (n = 5).

bone layer in the AOM scaffold. These results indicated that the AOM scaffold could regulate biphasic tissue-specific differentiations in different layers by mimicking chondrogenic and osteogenic biomimetic microenvironments.

Furthermore, RNA-seq analysis was performed to reveal the potential mechanisms during the chondrogenic and osteogenic differentiations of the BMSCs regulated by AOM scaffold. As shown in Fig. 6, for chondrogenic induction, the results showed that 2966 DEGs were detected

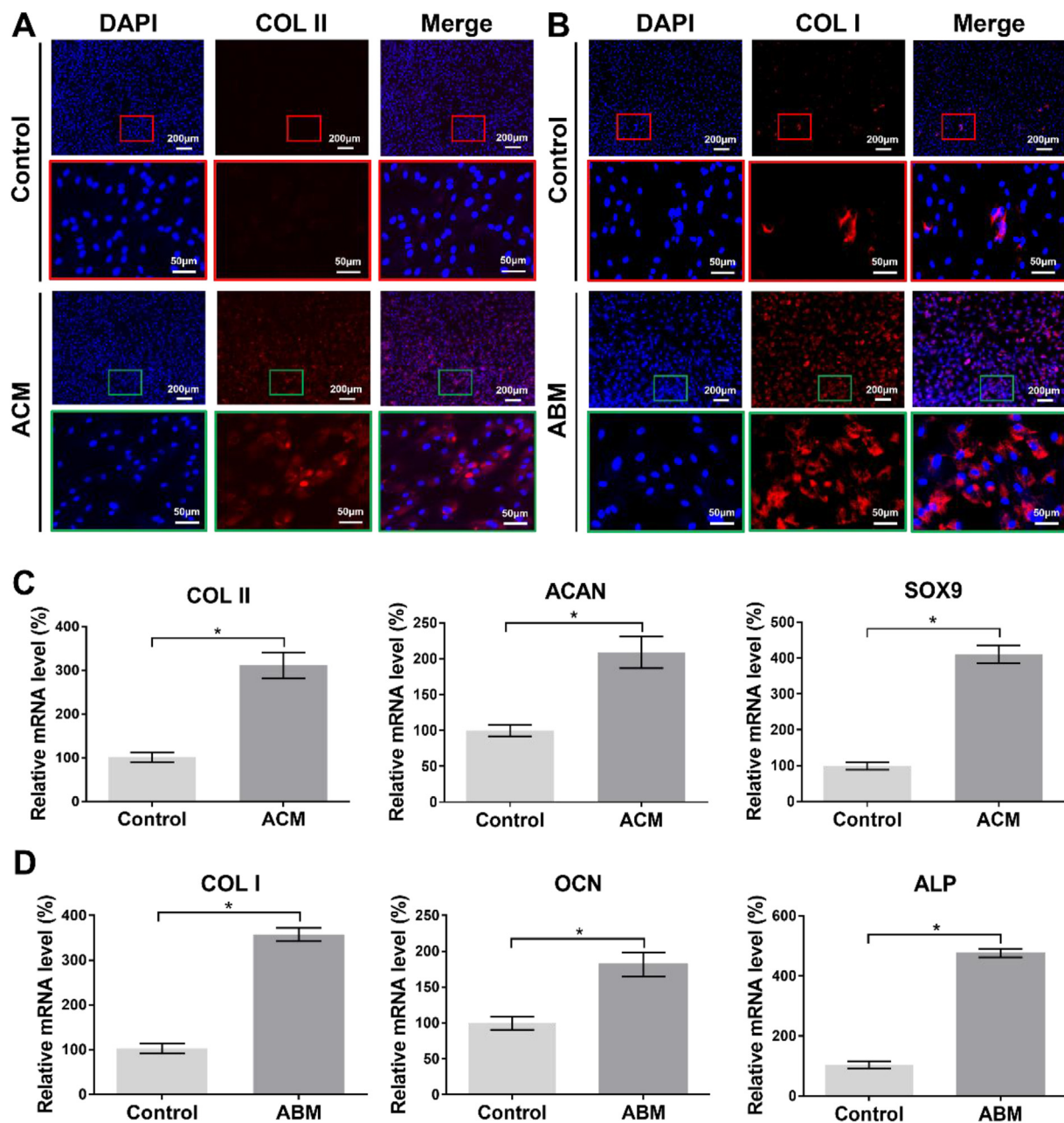


**Fig. 5.** *In vitro* tissue-specific differentiations of BMSCs mediated by the components of the AOM scaffold. (A) Immunofluorescence staining (red: COL II; blue: DAPI) of COL II induced by ACM powder derived from the AOM scaffold. (B) Immunofluorescence staining (red: COL I; blue: DAPI) of COL I induced by ABM powder derived from the AOM scaffold. (C) Expression of cartilage-specific genes (COL II, ACAN, and SOX9) induced by ACM powder. (D) Expression of bone-specific genes (COL I, ALP, and OCN) induced by ABM powder. (n = 4).

after culture in the ACM-added medium, with 1286 genes up-regulated and 1680 genes down-regulated (Fig. 6B1). KEGG pathway analysis and GO functional enrichment of up-regulated DEGs results (Fig. 6C1, D1, Table S2A) found that several cartilage-related pathways and bioprocesses, as well as cartilage-specific genes (COL II, ACAN, and SOX9), were significantly activated, such as the MAPK signaling pathway [51–53], cartilage development, glycosaminoglycan biosynthetic process, and negative regulation of smooth muscle cell proliferation. These signaling pathways, bioprocesses, and specific genes were related to the positive regulation of the chondrogenic differentiation, cartilage development, ECM synthesis, and negative regulation of angiogenesis, implying that ACM powder promoted chondrogenic differentiation and cartilage regeneration of BMSCs and inhibited the development of blood vessel, which benefited enhancing the stability of BMSC-regenerated

cartilage.

For osteogenic induction mediated by the ABM-added medium, 1188 genes were differentially expressed with 578 genes up-regulated and 610 genes down-regulated (Fig. 6B2). The KEGG and GO functional enrichment of up-regulated DEGs results (Fig. 6C2, D2, Table S2B) showed that several bone-related pathways and bioprocesses, as well as bone-specific genes (COL I and ALP), were significantly activated, such as AMPK signaling pathway [54,55], regulation of vascular associated smooth muscle cell proliferation, and canonical Wnt signaling pathway [56], which are highly related to osteogenic differentiation of BMSCs and regulation of angiogenesis. These results implied that ABM powder likely promoted bone regeneration by up-regulating osteogenesis- and angiogenesis-related signaling pathways, bioprocesses, and specific genes.

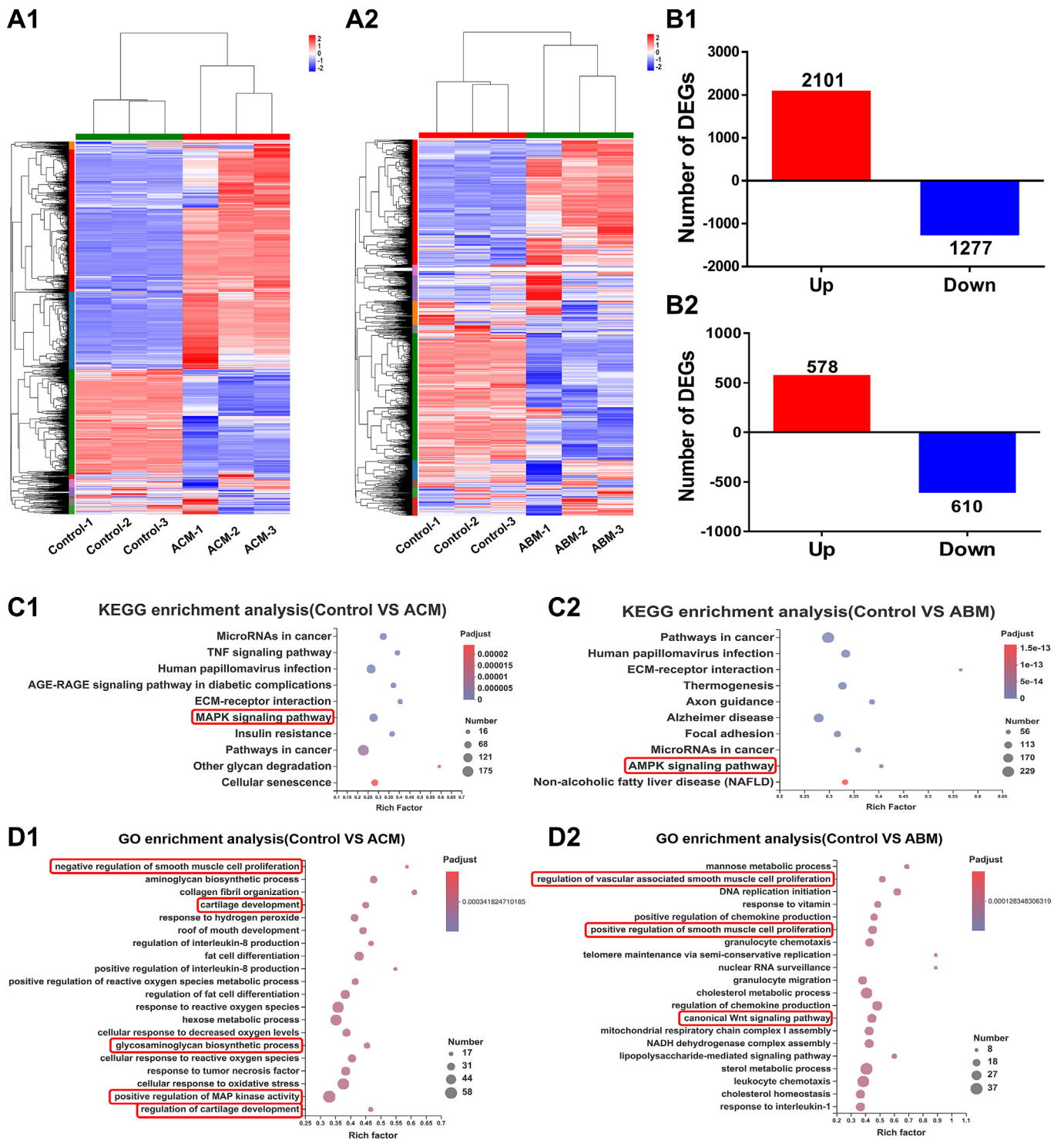


**Fig. 6.** The potential mechanism analysis of tissue-specific differentiation of BMSCs mediated by the components of the AOM scaffold. The (A1) heatmap, (B1) number, (C1) KEGG enrichment analysis (for up-regulated genes), and (D1) GO enrichment analysis (for up-regulated genes) of DEGs between the Control group and ACM group. The (A2) heatmap, (B2) number, (C2) KEGG enrichment analysis (for up-regulated genes), and (D2) GO enrichment analysis (for up-regulated genes) of DEGs between the Control group and ABM group. The terms in the red rectangle represent the signaling pathways and bioprocesses highly related to chondrogenic and osteogenic differentiation of BMSCs.

### 3.4. Tissue-specific repair of osteochondral defects mediated by the AOM scaffolds and BMSC-laden GelMA hydrogel

Tissue-specific repair of osteochondral defects mediated by AOM scaffolds and BMSC-laden GelMA hydrogel was evaluated in a knee joint model of rabbit (Fig. 7A1-A3). As shown in Fig. 7, gross view and micro-

CT images showed that obvious defects with fibrous-like tissue in both cartilage and bone regions were observed in the Untreated group at 6 weeks and 12 weeks post-implantation (Fig. 7B1, B4). In the Control group, the cartilage defects were distinctly observed with repair of fibrous-like tissue at 6 weeks (Fig. 7B2) and the defects had obvious shrinkage with little cartilage-like tissue regeneration at the edges of the

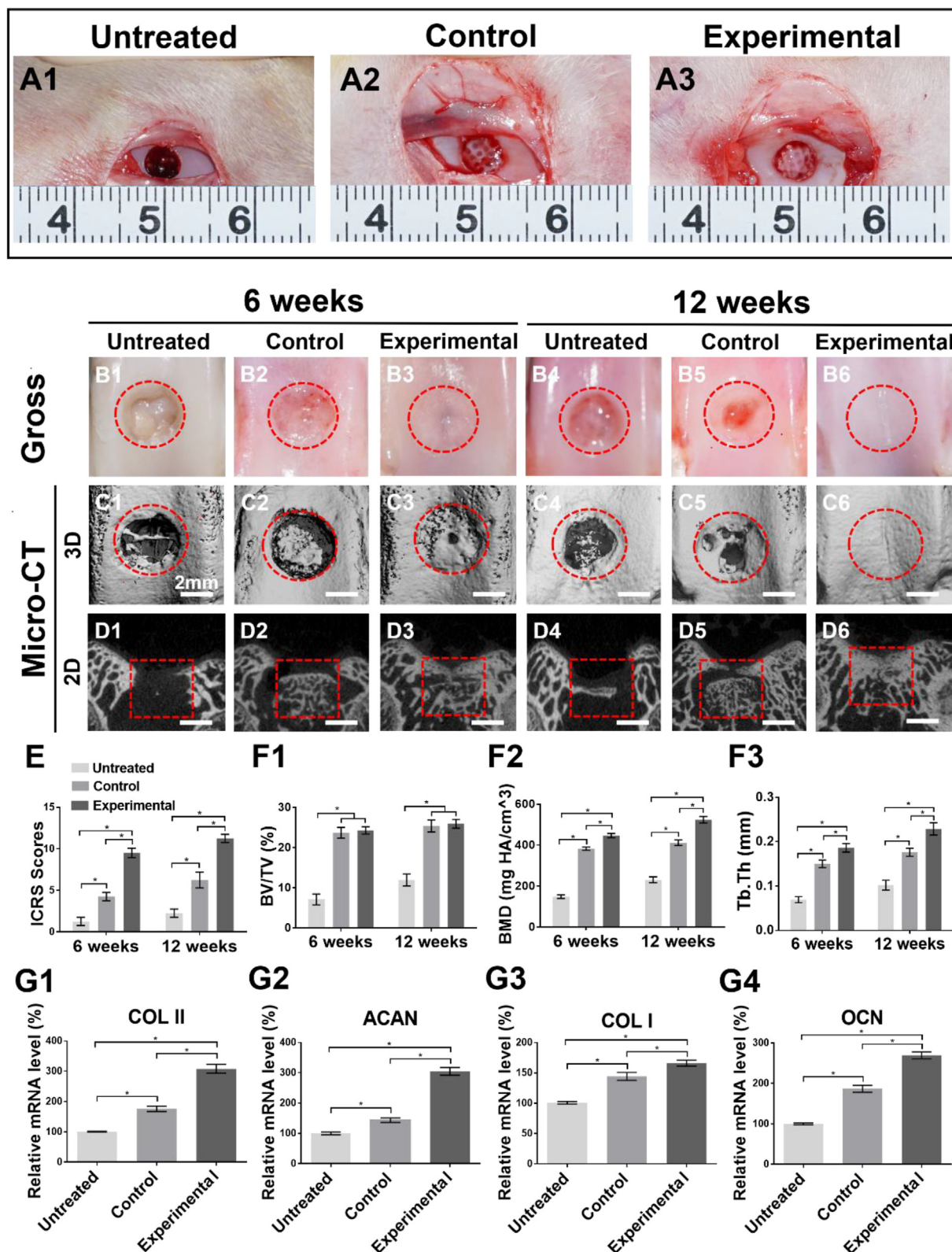


**Fig. 7.** Gross observation, micro-CT analysis, and related gene expression of osteochondral tissue-specific repair. (A1–A3) Rabbit knee joint surgery images. (B1–B6) Gross observation at 6 weeks and 12 weeks post-implantation. Micro-CT (C1–C6) 3D reconstructed images and (D1–D6) 2D cross-sectional images at 6 weeks and 12 weeks post-implantation. (E) ICRS macroscopic score of cartilage repair. (F1) BV/TV, (F2) BMD, and (F3) Tb. Th quantitative analyses of micro-CT. (G1–G4) Expression of cartilage-specific genes (COL II, ACAN) and bone-specific genes (COL I, OCN) at 12 weeks post-implantation. (n = 4).

defect at 12 weeks (Fig. 7B5). Micro-CT showed that the bone defects in the Control group were partially repaired by the implanted AOM scaffolds with inferior bone integration with surrounding native bone at both 6 weeks and 12 weeks (Fig. 7D2, D5). Excitingly, in the Experimental group, both cartilage and bone defects were satisfactorily repaired by cartilage-like tissue (Fig. 7B3, B6) at the cartilage defect regions and bone-like tissue at the bone defect regions with seamless integration with surrounding tissue (Fig. 7D3, D6) at both 6 weeks and 12 weeks. Differently, the defect regions presented a relatively rough surface and the partial residual of the AOM scaffold were observed at 6 weeks while the defect regions presented a relatively smooth surface and almost no residual of the AOM scaffold at 12 weeks (Fig. 7D3, D6).

Quantitative analyses demonstrated that the ICRS macroscopic scores (Fig. 7E), bone mineral density (BMD), trabecular thickness (Tb. Th), cartilage-specific gene expression (Fig. 7G1, G2), and bone-specific gene expression (Fig. 7G3, G4) significantly increased in order of the Untreated group, Control group, and Experimental group, indicating the best cartilage and bone regeneration in the Experimental group. Surprisingly, no significant differences were observed in bone volume fraction (BV/TV) between the Control and Experimental groups (Fig. 7F1), which was probably attributed to the abundant residual of the AOM scaffold with slower degradation rate in the Control group because of the lack of sufficient BMSCs to support bone remodeling.

Histological examinations further confirmed that the defects in the Untreated group were mainly repaired by fibrous tissue with an obvious gap between the defect regions and adjacent normal tissue (Fig. 8; Figure S3, S4). The repair of bone was improved in the implantation period from 6 weeks to 12 weeks (Fig. 8; Figure S3). However, the repair of cartilage effect was still poor at 12 weeks post-implantation (Fig. 8; Figure S3). The cartilage regions of the defect in the Control group were also repaired by fibrous tissue, except for a small amount of cartilage regeneration at the edges of the defect adjacent to normal tissue where a distinct boundary was observed (Fig. 8; Figure S3, S4). Consistent with micro-CT, abundant un-degraded AOM scaffolds were observed in the bone defect regions of the Control group, which was evidenced by

abundant acellular trabecular structures (Fig. 8; Figure S3, S4). Consistent with the gross view and micro-CT images, the cartilage defect regions in the Experimental group were mainly repaired by the regenerated cartilaginous tissue with a relatively smooth cartilage surface, relatively normal articular cartilage thickness, specific ECM staining, and seamless boundary healing between the neocartilage and surrounding native cartilage (Fig. 8; Figure S3, S4). The regions of COLII (for cartilage-specific protein) and COLI (for bone-specific protein) positively stained were generally consistent with those in S-F and M-T staining (Fig. 8; Figure S3, S4). For the repair of cartilage layer defects, the arrangement of chondrocytes was similar to that of native hyaline cartilage, which was showed that positive COLII staining and negative COLI staining (Fig. 8). Moreover, the neocartilage showed gradual maturation from 6 weeks to 12 weeks (Fig. 8; Figure S3). Additionally, the bone defect regions in the Experimental group mainly showed immature bony tissue and an incompletely degraded acellular bone layer of the AOM scaffold at 6 weeks, which was repaired by the relatively mature bony tissue with nearly no acellular bone layer residue of the AOM scaffold at 12 weeks. The regenerated bone showed typical morphological characteristics of subchondral bone (Fig. 8), and it was worth pointing out that the structure of tide line performed better reconstructed (Figure S4) in the Experimental group than that in the Control group and the Untreated group, which was likely attributed to the osteochondral interface (tide line) was not damaged during the preparation of AOM scaffolds and the regulated by the surrounding microenvironment (AOM scaffold and *in situ* microenvironment of the knee joint). The O'Driscoll histological assessment scores in the Experimental group were significantly greater than those in the Untreated and Control groups (Figure S5).

#### 4. Discussion

Although osteochondral tissue engineering has achieved some progress in animal models [57], it was hard to prepare a biphasic scaffold with accurate osteochondral-biomimetic microenvironment and interface similar to native articular tissue. To solve this problem, a double-layer

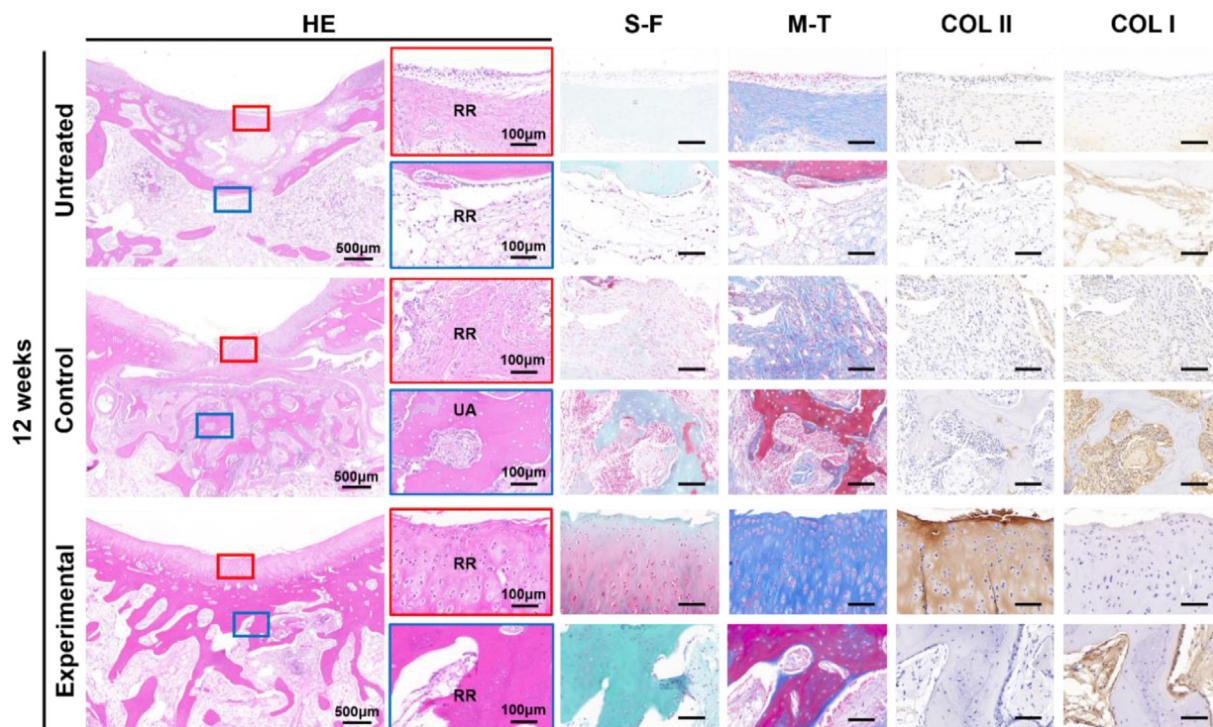


Fig. 8. Histological examinations of the regenerated osteochondral tissues at 12 weeks post-implantation. HE, Safranin O-Fast green (S-F), Masson's-Trichrome (M-T), COL II, and COL I staining show that tissue-specific structure and ECM deposition in both cartilage and bone defect regions of the Experimental group are very close to native articular osteochondral tissue, and were superior to those of the Untreated and Control groups. RR: regenerative region; UA: undegraded AOM.

AOM scaffold with natural osteochondral-biomimetic microenvironment and interface was successfully prepared in the current study. GelMA hydrogel was further used as the cell carrier to significantly enhance the efficiency of cell seeding and the homogeneity of cell distribution on the AOM scaffold. Meanwhile, *in vitro* results demonstrated that the chondrogenic/osteogenic components of the AOM scaffold efficiently regulated the differentiation of BMSCs by activating the chondrogenic/osteogenic-related pathways. Finally, the AOM scaffolds combined with BMSC-laden GelMA hydrogel successfully realized tissue-specific repair of the osteochondral defects with engineered cartilage and subchondral bone in a knee joint model of rabbit. These results provided a novel biomimetic scaffold and feasible strategy for the repair of osteochondral defects in the future.

How to prepare a porous AOM scaffold with natural osteochondral-biomimetic microenvironment and interface was the first problem that needed to be solved. The main difficulties were how to achieve successful acellularization and how to produce an acellular porous cartilage layer of natural osteochondral tissue suitable for cell loading, while ensuring the osteochondral interface was not damaged so as to maintain the relative dependence of chondrogenic and osteogenic microenvironments. Previous studies reported that CO<sub>2</sub> laser combined with decellularization technologies could be used to prepare cartilage tissue into an acellular porous scaffold with V-shaped micropore structures suitable for decellularization and cell loading [33]. However, the size (diameter and depth) of each V-shaped CO<sub>2</sub> laser micropore was relatively inconsistent under the same laser parameters, and easily led to low porosity, while the deeper V-shaped micropores for enhancing the porosity inevitably further decreased the consistency of the micropore size and increased the risk of osteochondral interface damage. Additionally, the high heat of the CO<sub>2</sub> laser likely compromised the bioactivity of the treated tissue and carbonized the treated tissue to increase the risk of harmful residual substance. To solve the above problems, UV picosecond laser technology with low heat was used to prepare a cartilage layer scaffold with U-shaped micropores, which efficiently enhanced the porosity, decreased the risk of tissue carbonization, and ensured the consistency of the micropore shape. The current results showed that the 15 laser repeats combined with decellularized treatment obtained a relatively optimized porous structure of the cartilage layer in the AOM scaffold, which had high mechanical strength (approximately 8.3 MPa) suitable for surgical operation and immediate functional maintenance, appropriate micropore interval for complete decellularization, accurate micropore depth close to, but did not damage, the interface, and sufficient space to ensure a high porosity for cell loading. In addition, no obvious carbonization was observed in the AOM scaffolds.

After the AOM scaffold were successfully prepared, how to achieve high cell seeding efficiency became an intractable problem. Direct seeding of the cell suspension easily led to a large amount of cell loss from the AOM scaffold because of the oversized pores (both the artificial micropores in the cartilage layer and the native bone trabecular interval in the bone layer), as shown in the Control group. Previous studies addressed this problem by increasing the chondrocyte density (up to  $2.0 \times 10^8$  cells/ml) to enhance the viscosity of the cell suspension [33]. Obviously, such high cell density is relatively difficult for practical clinical applications because of the high cost. To solve this problem, GelMA hydrogel was introduced as a cell carrier, which had excellent fluidity benefiting cell suspension and homogeneous seeding into the AOM scaffold before exposure to 365 nm light, and GelMA hydrogel was then fast gelation benefiting the firm fixation and homogenous distribution of cells in the AOM scaffold after exposure to 365 nm light. The results confirmed the feasibility of this strategy with high cell seeding efficiency, homogeneous cell distribution, and sustained proliferation, which ensured sufficient BMSCs for *in vivo* tissue-specific regeneration directed by the chondrogenic and osteogenic microenvironments of the AOM scaffold.

After successfully achieving a high cell seeding efficiency, whether the AOM scaffold has the ability for tissue-specific osteochondral

induction became another important issue. The current results demonstrated that the ACM and ABM powders from the AOM scaffold could significantly up-regulate the chondrogenic and osteogenic gene expression of BMSCs, respectively, indicating the tissue-specific regulation of AOM scaffold. To further clarify the potential mechanism during the AOM scaffold regulated chondrogenic and osteogenic differentiations of BMSCs, functional enrichment analysis of the up-regulated differential genes was performed to compare the differences in each group. The current results showed that the addition of ACM powder efficiently activated chondrogenic-related signaling pathways and bioprocesses, which was conducive to the chondrogenic differentiation of BMSCs, the secretion of ECM, and the prevention of the disordered growth of blood vessels in cartilage tissue during the *in vivo* cartilage layer defect repair. In addition, the addition of ABM powder also efficiently activated osteogenic signaling pathways and bioprocesses related to the osteogenic differentiation of BMSCs and the positive regulation of vascular ingrowth, which was likely conducive to accelerating bone remodeling during the *in vivo* bone defect repair. These results sufficiently confirmed the regulation roles of AOM scaffold on the osteochondral tissue-specific differentiation and further investigated the activated pathway during tissue-specific differentiation, which provided a reasonable explanation for the tissue-specific regeneration of the knee joint defect in the rabbit model.

Finally, whether the AOM scaffolds combined with BMSC-laden GelMA hydrogel can achieve satisfactory repair of osteochondral defects was the most concerned issue for future clinical translation. The current results confirmed that the blank group mainly exhibited misplaced fibrous tissue repair because of the lack of scaffold guidance and sufficient cell source. The Control group achieved partial osteochondral regeneration in the edge regions of the defect, which should benefit from endogenous stem cell homing and their tissue-specific regeneration directed by the chondrogenic and osteogenic microenvironment of AOM scaffold *in situ*. Nevertheless, the central regions of the osteochondral defects did not achieve satisfactory tissue-specific repair, which was likely due to insufficient cells from endogenous stem cell homing. In addition, the interface of the AOM scaffold and GelMA hydrogel might block the influx of bone marrow blood containing stem cells in the cartilage layer, leading to fibrous tissue formation in the central regions of the cartilage layer defects. Excitingly, the Experimental group achieved relatively satisfactory tissue-specific repair of the osteochondral defects with a relatively smooth cartilage surface, relatively mature osteochondral tissue, and an interface similar to a native interface, which was likely attributed to the following reasons: 1) The natural structure and mechanical support of the AOM scaffold provided a guide for early osteochondral tissue regeneration and avoided damage to the early tissue; 2) Abundant BMSCs (immobilized by GelMA hydrogel) achieved tissue-specific differentiation directed by the corresponding chondrogenic and osteogenic microenvironments of the AOM scaffold after implantation; 3) The natural interface of the AOM scaffold prevented excessive growth of the blood vessels toward cartilage region and maintained the relatively independent microenvironments of chondrogenesis and osteogenesis; 4) The *in situ* microenvironment of the knee joint (such as mechanical stress during articular movements) promoted tissue-specific differentiation and maturation of implanted autologous BMSCs. All of these results demonstrated that the microenvironment biomimetic AOM scaffold combined with BMSC-laden GelMA hydrogel was a satisfactory strategy for tissue-specific repair of osteochondral defect.

To facilitate easier access to scaffold materials and facilitate clinical translation, we manufactured xenogeneic (pig) AOM scaffold materials to repair rabbit osteochondral defects. Although the current research has achieved relatively satisfactory repair for osteochondral defects, it was difficult to trim the thickness of porcine articular cartilage to be the same as that of rabbit cartilage. Moreover, the natural articular cartilage had a non-homogenous structure (such as collagen fiber thickness, GAG content, and other ECM proteins) in different zones. The trim of sample

would destroy the natural non-homogenous structure. In addition, due to the huge size difference between pigs and rabbits, the cartilage-bone surface thickness would be very different. To avoid the above problems, preclinical large animal models (such as porcine model, whose articular size and cartilage thickness were very close to human) should be performed in future studies, which have been under investigation.

## 5. Conclusion

In summary, the current study developed a novel double-layer biomimetic scaffold with natural chondrogenic and osteogenic microenvironments as well as an interface. The AOM scaffolds combined with BMSC-laden GelMA hydrogel successfully repaired osteochondral defects with a relatively smooth cartilage surface, relatively mature osteochondral tissue, and an interface similar to natural tissue. Although other concerned clinical issues (such as biosafety of the AOM scaffold and osteochondral defect repair in a large animal model) remain to be addressed, the current results provided strong support for osteochondral tissue-specific repair and its future clinical translation.

## Credit author statement

Tao Wang, Wei Xu, and Xintong Zhao provided the concept of this research, conducted experimental design and completed most of the experiments. Baoshuai Bai and Yuejie Hua completed data sorting and analysis work. Jincheng Tang and Feifan Chen framed the figures and wrote the original draft of the article. Yu Liu refined the entire manuscript. Yahui Wang, Guangdong Zhou, and Yilin Cao supervised the whole study and obtained funding support for this research.

## Declaration of competing interest

The authors declare that they have no known competing financial interests or personal relationships that could have appeared to influence the work reported in this paper.

## Acknowledgment

This research was financially supported by the National Key Research and Development Program of China (2017YFC1103900, 2018YFC1105800), the National Natural Science Foundation of China (81871502, 81701843, and 81671837), the Program of Shanghai Academic/Technology Research Leader (19XD1431100), the Shanghai Collaborative Innovation Program on Regenerative Medicine and Stem Cell Research (2019CXJQ01), and the Clinical Research Plan of SHDC (No. SHDC2020CR2045B).

## Appendix A. Supplementary data

Supplementary data to this article can be found online at <https://doi.org/10.1016/j.mtbio.2022.100234>.

## References

- [1] A. Gobbi, G. Karnatzikos, A. Kumar, Long-term results after microfracture treatment for full-thickness knee chondral lesions in athletes, *Knee Surgery, Sport, Traumatol. Arthrosc.* 22 (2014) 1986–1996, <https://doi.org/10.1007/s00167-013-2676-8>.
- [2] M. Redondo, A. Beer, A. Yanke, Cartilage restoration: microfracture and osteochondral autograft transplantation, *J. Knee Surg.* 31 (2018) 231–238, <https://doi.org/10.1055/s-0037-1618592>.
- [3] G. Pipino, S. Risitano, F. Alviano, E.J. Wu, L. Bonsi, D.C. Vaccarisi, P.F. Indelli, Microfractures and hydrogel scaffolds in the treatment of osteochondral knee defects: a clinical and histological evaluation, *J. Clin. Orthop. Trauma.* 10 (2019) 67–75, <https://doi.org/10.1016/j.jcot.2018.03.001>.
- [4] G.M. Salzmann, M. Sauerchnig, M.T. Berninger, T. Kaltenhauser, M. Schönfelder, S. Vogt, G. Wexel, T. Tischer, N. Sudkamp, P. Niemeyer, A.B. Imhoff, P.B. Schöttle, The dependence of autologous chondrocyte transplantation on varying cellular passage, yield and culture duration, *Biomaterials* 32 (2011) 5810–5818, <https://doi.org/10.1016/j.biomaterials.2011.04.073>.
- [5] J.D. Harris, R.A. Siston, X. Pan, D.C. Flanagan, Autologous chondrocyte implantation, *J. Bone Jt. Surgery-American* 92 (2010) 2220–2233, <https://doi.org/10.2106/JBJS.J.00049>.
- [6] D.L. Richter, J.A. Tanksley, M.D. Miller, Osteochondral autograft transplantation: a review of the surgical technique and outcomes, *Sports Med. Arthrosc.* 24 (2016) 74–78, <https://doi.org/10.1097/JSA.000000000000099>.
- [7] M. Marcacci, E. Kon, M. Delcogliano, G. Filardo, M. Busacca, S. Zaffagnini, Arthroscopic autologous osteochondral grafting for cartilage defects of the knee, *Am. J. Sports Med.* 35 (2007) 2014–2021, <https://doi.org/10.1177/0363546507305455>.
- [8] D.J. Huey, J.C. Hu, K.A. Athanasiou, Unlike bone, cartilage regeneration remains elusive, *Science (80-.)* 338 (2012) 917–921, <https://doi.org/10.1126/science.1222454>.
- [9] R. Williams, I.M. Khan, K. Richardson, L. Nelson, H.E. McCarthy, T. Anabelsi, S.K. Singhrao, G.P. Dowthwaite, R.E. Jones, D.M. Baird, H. Lewis, S. Roberts, H.M. Shaw, J. Dudhia, J. Fairclough, T. Briggs, C.W. Archer, Identification and clonal characterisation of a progenitor cell sub-population in normal human articular cartilage, *PLoS One* 5 (2010), e13246, <https://doi.org/10.1371/journal.pone.0013246>.
- [10] A.M. Haleem, C.R. Chu, Advances in tissue engineering techniques for articular cartilage repair, *Operat. Tech. Orthop.* 20 (2010) 76–89, <https://doi.org/10.1053/j.oto.2009.10.004>.
- [11] N. Mahmoudifar, P.M. Doran, Tissue engineering of human cartilage and osteochondral composites using recirculation bioreactors, *Biomaterials* 26 (2005) 7012–7024, <https://doi.org/10.1016/j.biomaterials.2005.04.062>.
- [12] S.P. Nukavarapu, D.L. Dorcenus, Osteochondral tissue engineering: current strategies and challenges, *Biotechnol. Adv.* 31 (2013) 706–721, <https://doi.org/10.1016/j.biotechadv.2012.11.004>.
- [13] A. Boffa, L. Solaro, A. Poggi, L. Andriolo, D. Reale, A. Di Martino, Multi-layer cell-free scaffolds for osteochondral defects of the knee: a systematic review and meta-analysis of clinical evidence, *J. Exp. Orthop.* 8 (2021) 1–16, <https://doi.org/10.1186/s40634-021-00377-4>.
- [14] R. D'Ambrosi, F. Valli, P. De Luca, N. Ursino, F.G. Uselli, Maioregen osteochondral substitute for the treatment of knee defects: a systematic review of the literature, *J. Clin. Med.* 8 (2019), <https://doi.org/10.3390/jcm8060783>.
- [15] L. Jia, Y. Zhang, L. Yao, P. Zhang, Z. Ci, W. Zhang, C. Miao, X. Liang, A. He, Y. Liu, S. Tang, R. Zhang, X. Wang, Y. Cao, G. Zhou, Regeneration of human-ear-shaped cartilage with acellular cartilage matrix-based biomimetic scaffolds, *Appl. Mater. Today.* 20 (2020) 100639, <https://doi.org/10.1016/j.apmt.2020.100639>.
- [16] Y. Chen, T. Wu, S. Huang, C.-W.W. Suen, X. Cheng, J. Li, H. Hou, G. She, H. Zhang, H. Wang, X. Zheng, Z. Zha, Sustained release SDF-1 $\alpha$ /TGF- $\beta$ 1-loaded silk fibroin-porous gelatin scaffold promotes cartilage repair, *ACS Appl. Mater. Interfaces* 11 (2019) 14608–14618, <https://doi.org/10.1021/acsami.9b01532>.
- [17] C. Antich, G. Jiménez, J. Vicente, E. López Ruiz, C. Chocarro Wrona, C. Grinán Lisón, E. Carrillo, E. Montañez, J.A. Marchal, Development of a biomimetic hydrogel based on predifferentiated mesenchymal stem-cell-derived ECM for cartilage tissue engineering, *Adv. Healthc. Mater.* 10 (2021) 2001847, <https://doi.org/10.1002/adhm.202001847>.
- [18] S. Wang, R. Gu, F. Wang, X. Zhao, F. Yang, Y. Xu, F. Yan, Y. Zhu, D. Xia, Y. Liu, A three-dimensional Zn/PCL scaffold for bone regeneration with a dose-dependent effect on osteogenesis and osteoclastogenesis, *Mater. Today Bio* (2022) 100202, <https://doi.org/10.1016/j.mtbio.2021.100202>.
- [19] S. Minardi, F. Taraballi, F.J. Cabrera, J. Van Eps, X. Wang, S.A. Gazze, J.S. Fernandez-Mourey, A. Tampieri, L. Francis, B.K. Weiner, E. Tasciotti, Biomimetic hydroxyapatite/collagen composite drives bone niche recapitulation in a rabbit orthotopic model, *Mater. Today Bio.* 2 (2019) 100005, <https://doi.org/10.1016/j.mtbio.2019.100005>.
- [20] W.-H. Wang, F. Wang, H.-F. Zhao, K. Yan, C.-L. Huang, Y. Yin, Q. Huang, Z.-Z. Chen, W.-Y. Zhu, Injectable magnesium-zinc alloy containing hydrogel complex for bone regeneration, *Front. Bioeng. Biotechnol.* 8 (2020), <https://doi.org/10.3389/fbioe.2020.617585>.
- [21] Z.-K. Cui, S. Kim, J.J. Baljon, B.M. Wu, T. Aghaloo, M. Lee, Microporous methacrylated glycol chitosan-montmorillonite nanocomposite hydrogel for bone tissue engineering, *Nat. Commun.* 10 (2019), <https://doi.org/10.1038/s41467-019-11511-3>.
- [22] C. Deng, H. Zhu, J. Li, C. Feng, Q. Yao, L. Wang, J. Chang, C. Wu, Bioactive scaffolds for regeneration of cartilage and subchondral bone interface, *Theranostics* 8 (2018) 1940–1955, <https://doi.org/10.7150/thno.23674>.
- [23] N. Mohan, N.H. Dormer, K.L. Caldwell, V.H. Key, C.J. Berklund, M.S. Detamore, Continuous gradients of material composition and growth factors for effective regeneration of the osteochondral interface, *Tissue Eng. Part A.* 17 (2011) 2845–2855, <https://doi.org/10.1089/ten.tea.2011.0135>.
- [24] N.T. Khanarian, N.M. Haney, R.A. Burga, H.H. Lu, A functional agarose-hydroxyapatite scaffold for osteochondral interface regeneration, *Biomaterials* 33 (2012) 5247–5258, <https://doi.org/10.1016/j.biomaterials.2012.03.076>.
- [25] M. Joseph Christakiran, P.J.T. Reardon, R. Konwarh, J.C. Knowles, B.B. Mandal, Mimicking hierarchical complexity of the osteochondral interface using electrospun silk-bioactive glass composites, *ACS Appl. Mater. Interfaces* 9 (2017) 8000–8013, <https://doi.org/10.1021/acsami.6b16590>.
- [26] S.O. Sarrigiannidis, J.M. Rey, O. Dobre, C. González-García, M.J. Dalby, M. Salmeron-Sanchez, A tough act to follow: collagen hydrogel modifications to improve mechanical and growth factor loading capabilities, *Mater. Today Bio.* 10 (2021), <https://doi.org/10.1016/j.mtbio.2021.100098>.
- [27] W. Shi, M. Sun, X. Hu, B. Ren, J. Cheng, C. Li, X. Duan, X. Fu, J. Zhang, H. Chen, Y. Ao, Structurally and functionally optimized silk-fibroin-gelatin scaffold using 3D

- printing to repair cartilage injury in vitro and in vivo, *Adv. Mater.* 29 (2017) 1701089, <https://doi.org/10.1002/adma.201701089>.
- [28] F. Gao, Z. Xu, Q. Liang, H. Li, L. Peng, M. Wu, X. Zhao, X. Cui, C. Ruan, W. Liu, Osteochondral regeneration with 3D-printed biodegradable high-strength supramolecular polymer reinforced-gelatin hydrogel scaffolds, *Adv. Sci.* 6 (2019) 1900867, <https://doi.org/10.1002/adv.201900867>.
- [29] X. Zhu, T. Chen, B. Feng, J. Weng, K. Duan, J. Wang, X. Lu, Biomimetic bacterial cellulose-enhanced double-network hydrogel with excellent mechanical properties applied for the osteochondral defect repair, *ACS Biomater. Sci. Eng.* 4 (2018) 3534–3544, <https://doi.org/10.1021/acsbomaterials.8b00682>.
- [30] J. Zhao, A. Kirillova, C.N. Kelly, H. Xu, W.J. Koshut, F. Yang, K. Gall, B.J. Wiley, High-strength hydrogel attachment through nanofibrous reinforcement, *Adv. Healthc. Mater.* 10 (2021) 2001119, <https://doi.org/10.1002/adhm.202001119>.
- [31] X. Sun, Y. Wang, Z. Guo, B. Xiao, Z. Sun, H. Yin, H. Meng, X. Sui, Q. Zhao, Q. Guo, A. Wang, W. Xu, S. Liu, Y. Li, S. Lu, J. Peng, Acellular cauda equina allograft as main material combined with biodegradable chitin conduit for regeneration of long-distance sciatic nerve defect in rats, *Adv. Healthc. Mater.* 7 (2018) 1800276, <https://doi.org/10.1002/adhm.201800276>.
- [32] B.B. Rothrauff, R.S. Tuan, Decellularized bone extracellular matrix in skeletal tissue engineering, *Biochem. Soc. Trans.* 48 (2020) 755–764, <https://doi.org/10.1042/BST20190079>.
- [33] Y. Li, Y. Xu, Y. Liu, Z. Wang, W. Chen, L. Duan, D. Gu, Decellularized cartilage matrix scaffolds with laser-machined micropores for cartilage regeneration and articular cartilage repair, *Mater. Sci. Eng. C* 105 (2019) 110139, <https://doi.org/10.1016/j.msec.2019.110139>.
- [34] Y.Y. Gong, J.X. Xue, W.J. Zhang, G.D. Zhou, W. Liu, Y. Cao, A sandwich model for engineering cartilage with acellular cartilage sheets and chondrocytes, *Biomaterials* 32 (2011) 2265–2273, <https://doi.org/10.1016/j.biomaterials.2010.11.078>.
- [35] F. Pati, J. Jang, D.H. Ha, S. Won Kim, J.W. Rhie, J.H. Shim, D.H. Kim, D.W. Cho, Printing three-dimensional tissue analogues with decellularized extracellular matrix bioink, *Nat. Commun.* 5 (2014) 1–11, <https://doi.org/10.1038/ncomms4935>.
- [36] J. Yin, M. Yan, Y. Wang, J. Fu, H. Suo, 3D bioprinting of low-concentration cell-laden gelatin methacrylate (GelMA) bioinks with a two-step cross-linking strategy, *ACS Appl. Mater. Interfaces* 10 (2018) 6849–6857, <https://doi.org/10.1021/acsaami.7b16059>.
- [37] A.I. Van Den Bulcke, B. Bogdanov, N. De Rooze, E.H. Schacht, M. Cornelissen, H. Berghmans, Structural and rheological properties of methacrylamide modified gelatin hydrogels, *Biomacromolecules* 1 (2000) 31–38.
- [38] B.D. Fairbanks, M.P. Schwartz, C.N. Bowman, K.S. Anseth, Photoinitiated polymerization of PEG-diacrylate with lithium phenyl-2,4,6-trimethylbenzoylphosphine: polymerization rate and cytocompatibility, *Biomaterials* 30 (2009) 6702–6707, <https://doi.org/10.1016/j.biomaterials.2009.08.055>.
- [39] Y. Wang, Y. Xu, G. Zhou, Y. Liu, Y. Cao, Biological evaluation of acellular cartilaginous and dermal matrices as tissue engineering scaffolds for cartilage regeneration, *Front. Cell Dev. Biol.* 8 (2021), <https://doi.org/10.3389/fcell.2020.624337>.
- [40] Y. Hua, H. Xia, L. Jia, J. Zhao, D. Zhao, X. Yan, Y. Zhang, S. Tang, G. Zhou, L. Zhu, Q. Lin, Ultrafast, tough, and adhesive hydrogel based on hybrid photocrosslinking for articular cartilage repair in water-filled arthroscopy, *Sci. Adv.* 7 (2021), <https://doi.org/10.1126/sciadv.abg0628>.
- [41] D. Gan, Z. Wang, C. Xie, X. Wang, W. Xing, X. Ge, H. Yuan, K. Wang, H. Tan, X. Lu, Mussel-inspired tough hydrogel with in situ nanohydroxyapatite mineralization for osteochondral defect repair, *Adv. Healthc. Mater.* 8 (2019) 1901103, <https://doi.org/10.1002/adhm.201901103>.
- [42] H. Liu, J. Liu, C. Qi, Y. Fang, L. Zhang, R. Zhuo, X. Jiang, Thermosensitive injectable in-situ forming carboxymethyl chitin hydrogel for three-dimensional cell culture, *Acta Biomater.* 35 (2016) 228–237, <https://doi.org/10.1016/j.actbio.2016.02.028>.
- [43] D. Li, L. Zhu, Y. Liu, Z. Yin, Y. Liu, F. Liu, A. He, S. Feng, Y. Zhang, Z. Zhang, W. Zhang, W. Liu, Y. Cao, G. Zhou, Stable subcutaneous cartilage regeneration of bone marrow stromal cells directed by chondrocyte sheet, *Acta Biomater.* 54 (2017) 321–332, <https://doi.org/10.1016/j.actbio.2017.03.031>.
- [44] Z. Qiao, M. Lian, Y. Han, B. Sun, X. Zhang, W. Jiang, H. Li, Y. Hao, K. Dai, Bioinspired stratified electrowritten fiber-reinforced hydrogel constructs with layer-specific induction capacity for functional osteochondral regeneration, *Biomaterials* 266 (2021) 120385, <https://doi.org/10.1016/j.biomaterials.2020.120385>.
- [45] R. Cao, A. Zhan, Z. Ci, C. Wang, Y. She, Y. Xu, K. Xiao, H. Xia, L. Shen, D. Meng, C. Chen, A biomimetic biphasic scaffold consisting of decellularized cartilage and decalcified bone matrixes for osteochondral defect repair, *Front. Cell Dev. Biol.* 9 (2021), <https://doi.org/10.3389/fcell.2021.639006>.
- [46] M.P.J. van den Borne, N.J.H. Raijmakers, J. Vanlauwe, J. Victor, S.N. de Jong, J. Bellemans, D.B.F. Saris, International cartilage repair society (ICRS) and oswestry macroscopic cartilage evaluation scores validated for use in autologous chondrocyte implantation (ACI) and microfracture, *Osteoarthritis Cartilage* 15 (2007) 1397–1402, <https://doi.org/10.1016/j.joca.2007.05.005>.
- [47] Y. Du, H. Liu, Q. Yang, S. Wang, J. Wang, J. Ma, I. Noh, A.G. Mikos, S. Zhang, Selective laser sintering scaffold with hierarchical architecture and gradient composition for osteochondral repair in rabbits, *Biomaterials* 137 (2017) 37–48, <https://doi.org/10.1016/j.biomaterials.2017.05.021>.
- [48] Y. Liu, L. Peng, L. Li, C. Huang, K. Shi, X. Meng, P. Wang, M. Wu, L. Li, H. Cao, K. Wu, Q. Zeng, H. Pan, W.W. Lu, L. Qin, C. Ruan, X. Wang, 3D-bioprinted BMSC-laden biomimetic multiphasic scaffolds for efficient repair of osteochondral defects in an osteoarthritic rat model, *Biomaterials* 279 (2021) 121216, <https://doi.org/10.1016/j.biomaterials.2021.121216>.
- [49] M. Torzewski, M. Klouche, J. Hock, M. Messner, B. Dorweiler, J. Torzewski, H.E. Gabbert, S. Bhakdi, Immunohistochemical demonstration of enzymatically modified human LDL and its colocalization with the terminal complement complex in the early atherosclerotic lesion, *Arterioscler. Thromb. Vasc. Biol.* 18 (1998) 369–378, <https://doi.org/10.1161/01.atv.18.3.369>.
- [50] S. O'Driscoll, F. Keeley, R. Salter, The Chondrogenic Periosteal Grafts Influence Potential for of Free Autogenous Resurfacing Surfaces Motion Biological Defects of Major under the in Joint Passive of Continuous, 1986, p. 68.
- [51] N. Ma, X. Teng, Q. Zheng, P. Chen, The regulatory mechanism of p38/MAPK in the chondrogenic differentiation from bone marrow mesenchymal stem cells, *J. Orthop. Surg. Res.* 14 (2019), <https://doi.org/10.1186/s13018-019-1505-2>.
- [52] M. Hou, Y. Zhang, X. Zhou, T. Liu, H. Yang, X. Chen, F. He, X. Zhu, Kartogenin prevents cartilage degradation and alleviates osteoarthritis progression in mice via the miR-146a/NRF2 axis, *Cell Death Dis.* 12 (2021), <https://doi.org/10.1038/s41419-021-03765-x>.
- [53] Y. Zhang, J. Li, M.E. Davis, M. Pei, Delineation of in vitro chondrogenesis of human synovial stem cells following preconditioning using decellularized matrix, *Acta Biomater.* 20 (2015) 39–50, <https://doi.org/10.1016/j.actbio.2015.04.001>.
- [54] Y. Wang, X. Qu, Y. Yang, X. Han, L. Wang, H. Qiao, Q. Fan, T. Tang, K. Dai, AMPK promotes osteogenesis and inhibits adipogenesis through AMPK-Gfi1-OPN axis, *Cell. Signal.* 28 (2016) 1270–1282, <https://doi.org/10.1016/j.cellsig.2016.06.004>.
- [55] J. Jeyabalan, M. Shah, B. Violette, C. Chenu, AMP-activated protein kinase pathway and bone metabolism, *J. Endocrinol.* 212 (2012) 277–290, <https://doi.org/10.1530/JOE-11-0306>.
- [56] C. Hartmann, A Wnt canon orchestrating osteoblastogenesis, *Trends Cell Biol.* 16 (2006) 151–158, <https://doi.org/10.1016/j.tcb.2006.01.001>.
- [57] W. Wei, H. Dai, Articular cartilage and osteochondral tissue engineering techniques: recent advances and challenges, *Bioact. Mater.* 6 (2021) 4830–4855, <https://doi.org/10.1016/j.bioactmat.2021.05.011>.